Positive isotropic components of the 2025 Santorini-Amorgos earthquakes

(report to EMSC submitted February 18, 2025)

J. Zahradník[1], E. Sokos[2], Z. Roumelioti[2], F. Turhan[3]
[1] Faculty of Mathematics and Physics, Charles University, Prague, Czech Republic (jiri.zahradnik@matfyz.cuni.cz)
[2] Department of Geology, University of Patras, Patras, Greece (esokos@upatras.gr, zroumelioti@upatras.gr)
[3] Kandilli Observatory and Earthquake Research Institute (KOERI), Regional Earthquake-Tsunami Monitoring Center (RETMC), Boğaziçi University, Istanbul, Türkiye (fatih.turhan@bogazici.edu.tr)

Summary. We used full waveforms of the Hellenic Unified Seismic Network (HUSN) regional stations and a frequency range of 0.03-0.06 Hz. We calculated full moment tensors (MTs) and focused on their ISO and CLVD components. In the tested depth range of 1-20 km, the medians of ISO (=VOL) and CLVD are positive, but their 68% confidence intervals are broad due to the tradeoff of the non-DC with depth. When constraining source depths to ≥ 7 km, indicated by relocations, MTs have unambiguously positive ISO and positive CLVD, pointing to a shear-opening source process.

Introduction. The current seismic activity near Amorgos Island may contribute to understanding the relative roles of tectonic, volcanic and magmatic processes in the region (e.g. Andinisari et al., 2021; Heath et al., 2019). Here we report on non-double-couple (non-DC) components of the full moment tensor (MT) of 19 events analyzed so far.

Method. We use semi-automatic station selection, starting from the deviatoric moment-tensor calculation of NOA with GISOLA (Triantafyllis et al., 2016 and 2022), http://orfeus.gein.noa.gr/gisola/realtime/2025/, and we adopt their pre-processed instrumentally corrected full waveforms. A typical set consists of ~ 8-15 stations of HUSN (Evangelidis et al. 2021) at epicentral distances from ~40 to ~300 km. Further, we use the manually revised epicenter location by NOA and set the trial source positions below the epicenter. Four 1D velocity models were tested, i.e., Brüstle, et al. (2012), Dimitriadis et al. (2010), Novotný et al. (2001), and Fountoulakis (personal communication). Results for the latter velocity model are presented below. All the tested models provide qualitatively the same results in the frequency range of 0.03-0.06 Hz. Full moment tensor is calculated with ISOLA2024 software (Zahradník and Sokos, 2018 and 2025) and its newer Bayesian bootstrap version enabling quantification of confidence intervals of the ISO and CLVD components. An example of the processing for the event of 2025-02-04 (13:04 UTC) is shown in Attachment, Figs. A1-A4.

Results. The full MTs are presented in Fig. 1a. Their waveform-preferred depths vary from 3 to 12 km. The results from the Bayesian bootstrap are presented in Table 1. First, we use trial source depths of 1-20 km (step 1 km). The table shows that the ISO median values of all events (except one low-quality inversion, No. 8) are positive. However, the 68% confidence intervals

of ISO and CLVD are relatively large. This effect is due to the tradeoff between non-DC components and depth. The zero-valued ISO and CLVD would be possible if the depth is shallower than ~7 km. In this light, fundamental improvement of the resolution of the non-DC components is provided using relocated hypocenters. We calculate them by hypoDD code (Waldhauser, 2000; Waldhauser and Ellsworth, 2000), see Table 1. Based on the relocations we performed the second set of inversions with depth constrained to 7-20 km. Then, as demonstrated in Fig. 1b, the waveform inversion unambiguously provides full MTs with ISO > 0 and CLVD > 0 (highlighted in bold in Table 1) thus pointing to a shear-tensile (opening) source process. For the theory of such earthquakes, see Vavryčuk (2011). Interpretation of the present observations will be provided elsewhere.

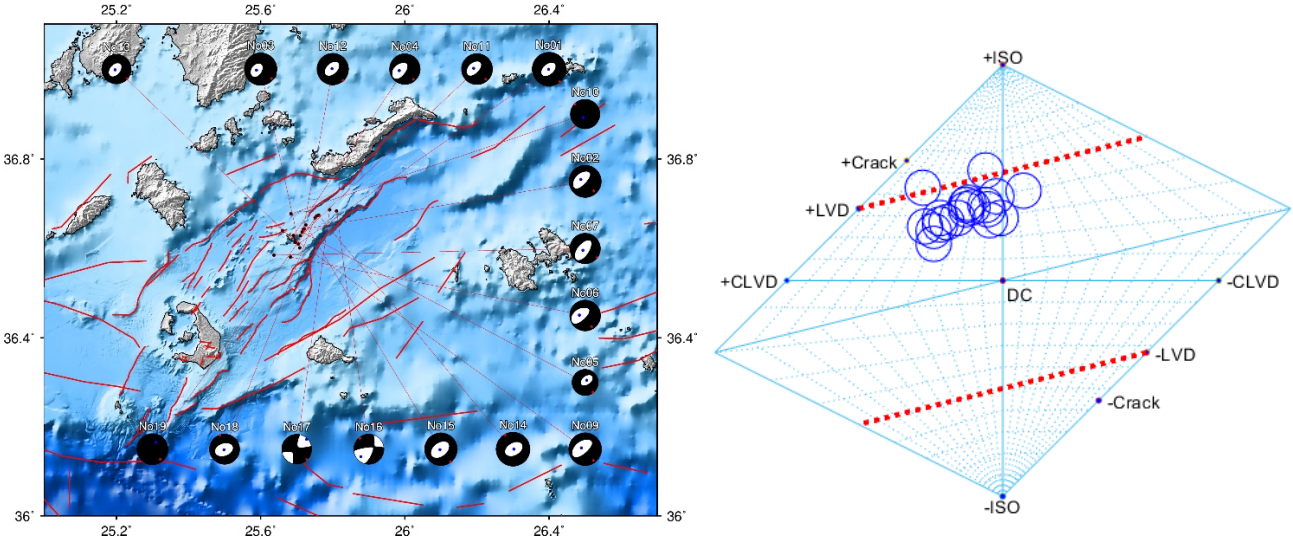

a) b)

Fig. 1. (a) Full MTs, topography and bathymetry from GEBCO (https://www.gebco.net/) and Hooft et al.,2023, fault lines from NOA FAULTS 6.0 (Ganas, 2023). (b) The source-type plot. The figures are based on median ISO and CLVD values obtained with depth constrained to 7-20 km.

Table 1. ISO and CLVD are given with their 15.87%, 50% (median), and 84.13% percentiles. No. is an internal numbering of events in this study. The line in gray corresponds to the low-quality inversion of event No. 8.

Date - Time	Mw	ISO (%) Depth 1-20 km	CLVD (%) Depth 1-20 km	ISO (%) Depth ≥ 7-20km	CLVD (%) Depth ≥ 7-20km	Relocated depths (km)
No01_2025/02/04_13:04:14.56	5.3	23 **35** 45	-2 15 27	24 **36** 46	-1 **16** 27	13.9
No02_2025/02/05_19:09:38.62	5.0	-21 24 40	-23 26 39	18 **29** 42	9 **29** 39	12.6
No03_2025/02/03_09:29:42.49	5.1	-24 16 53	-56 -21 16	19 **39** 58	-41 **3** 19	14.2
No04_2025/02/03_20:19:39.39	4.8	-15 21 39	-27 15 40	15 **29** 42	3 **21** 42	13.9
No05_2025/02/08_16:30:00.76	4.1	-32 2 41	-34 -2 28	19 **35** 51	-6 **17** 35	12.4
No06_2025/02/08_09:00:41.37	4.8	-15 14 39	-5 17 29	15 **27** 42	13 **26** 37	14.0
No07_2025/02/07_07:16:13.66	4.8	-5 20 42	3 30 48	12 **25** 44	16 **36** 50	12.2
No08_2025/02/02_23:54:41.58	4.9	-39 -23 -4	-32 -8 41	-43 **-26** -1	-38 **6** 56	12.0
No09_2025/02/09_19:05:39.41	5.1	0 22 31	9 25 35	16 **26** 34	22 **29** 37	11.6
No10_2025/02/05_17:47:28.04	4.6	-14 26 49	-19 5 30	43 **51** 60	-4 **8** 28	17.8
No11_2025/02/04_02:46:06.98	4.8	17 32 44	-4 16 32	18 **33** 45	-1 **17** 32	12.7
No12_2025/02/03_12:17:40.53	4.9	13 32 44	-7 13 28	18 **34** 46	-5 **14** 27	12.3
No13_2025/02/02_17:45:44.99	4.6	-15 25 44	-34 0 21	19 **35** 49	-12 **8** 24	13.2
No14_2025/02/10_20:16:29.37	5.3	-30 30 44	-35 3 20	16 **33** 45	-10 **7** 21	13.7
No15_2025/02/10_22:37:25.55	5.1	2 26 40	-18 5 19	13 **28** 43	-13 **6** 20	12.4
No16_2025/02/10_11:23:17.71	4.7	6 17 26	19 31 42	8 **17** 26	19 **32** 42	16.9
No17_2025/02/11_05:58:44.81	4.7	17 23 32	18 32 45	17 **23** 32	18 **32** 45	14.9
No18_2025/02/11_07:17:19.00	4.7	-19 25 45	-32 -3 13	8 **29** 45	-19 **1** 15	15.3
No19_2025/02/11_11:43:54.22	4.9	29 42 53	17 36 47	34 **43** 54	22 **37** 48	12.0

Attachment

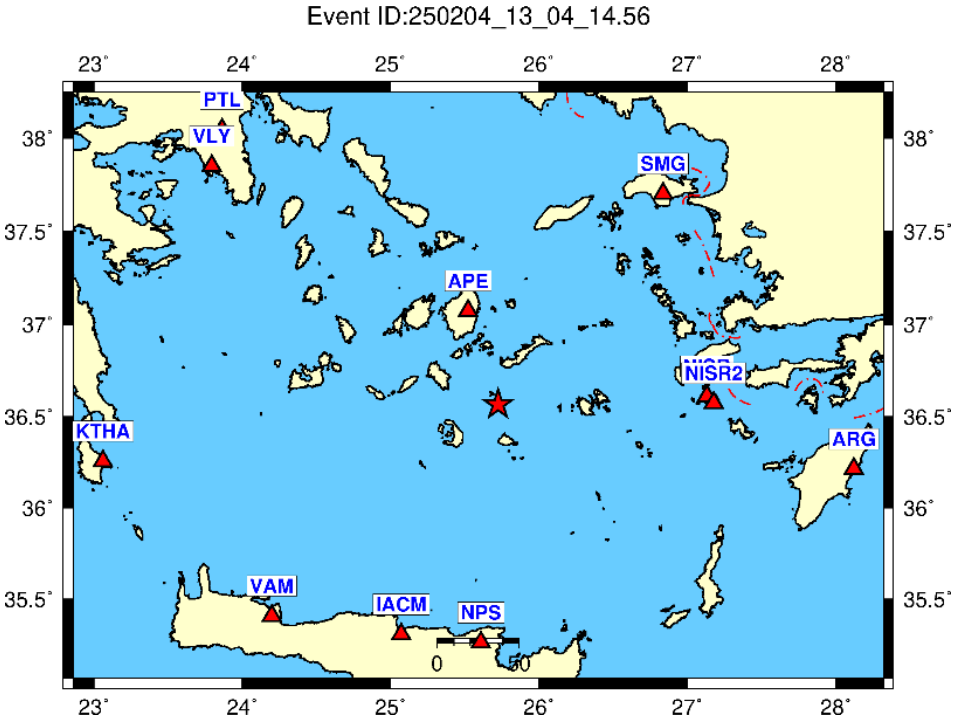

Fig. A1. Epicenter (star) of one of the events, No. 1, and used HUSN stations (triangles).

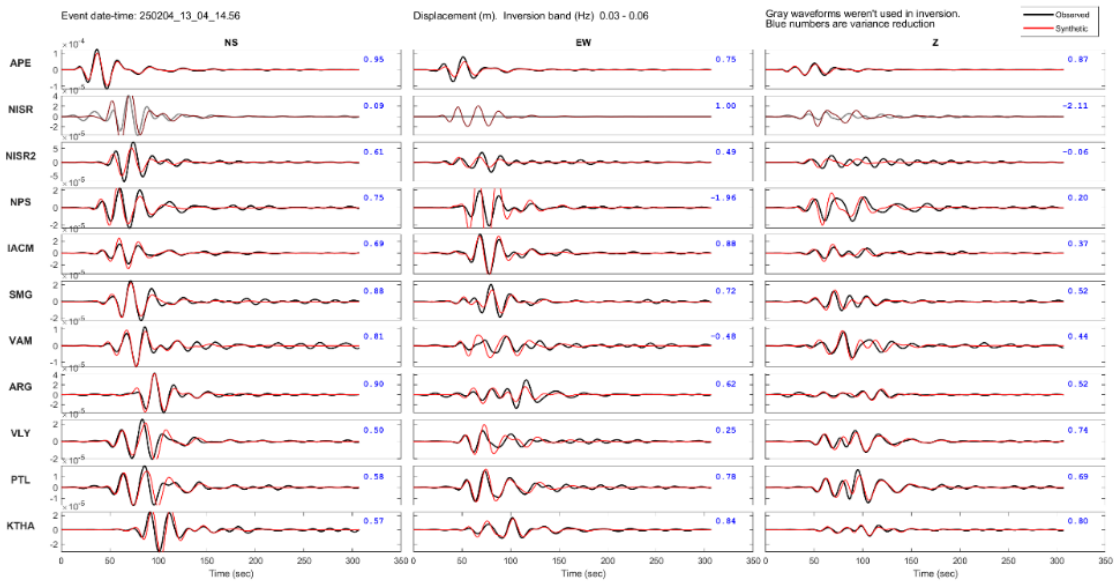

Fig. A2. Waveform fit.

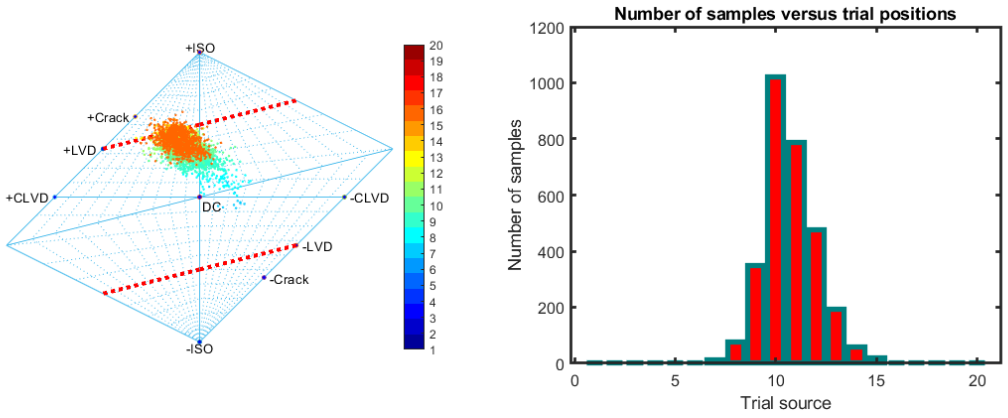

Fig. A3. Source type plot and depth preference from Isola2024 (positions 1-20 refer to depth 1-20 km). Dots in the source type plot, color-coded with trial depth, are random MT samples demonstrating uncertainty.

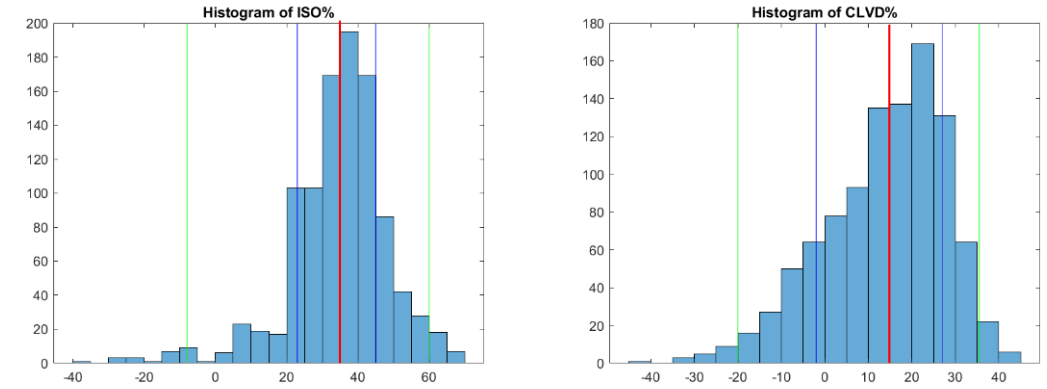

a) b)

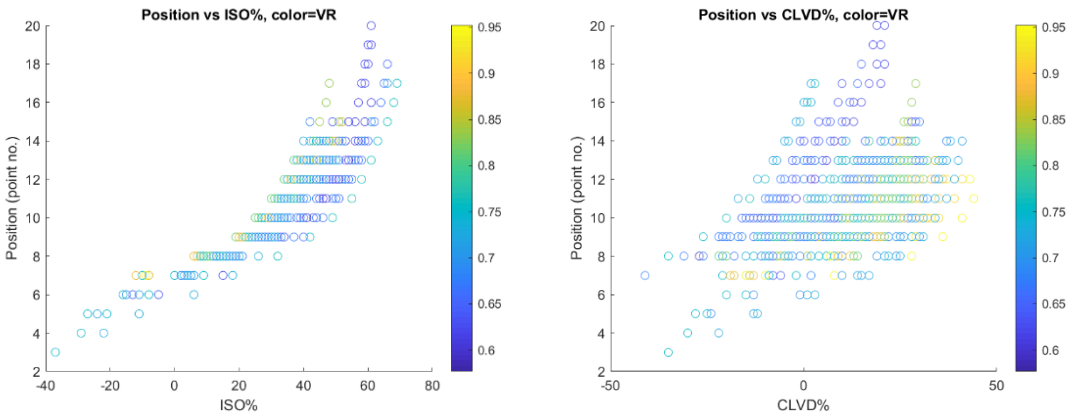

c) d)

Fig. A4. Non-DC components (ISO and CLVD)) and their uncertainty estimate from the bootstrap version of Isola (positions 1-20 refer to depth 1-20 km). Vertical lines in panels (a) and (b) are the percentiles, median is shown in red. Note ISO > 0 for depths > 7 km in panel (c). VR is variance reduction.

Data and Resources. Regional waveform data used in this study were obtained from the Hellenic Unified Seismic Network (HUSN) networks, HL, DOI:10.7914/SN/HL, HC, DOI:10.7914/SN/HC, HP, DOI:10.7914/SN/HP and HA, DOI:10.7914/SN/HA. Data from the HL, HC, HP, and HA networks can be accessed through the National Observatory of Athens (NOA) EIDA node https://eida.gein.noa.gr/ (Evangelidis et al., 2021). ISOLA software can be downloaded from https://geo.mff.cuni.cz/~jz/for_ISOLAnews/. The maps were generated using the Generic Mapping Tools v.6, https://www.generic-mapping-tools.org/download/.

Acknowledgments. The authors would like to thank I. Fountoulakis and C. Evangelidis for valuable discussions and for providing the local velocity model. We also thank A. Lomax for discussing with us his relocation results. Special thanks to all the Greek colleagues who are installing new instruments and processing all sorts of data during this remarkable sequence. Code sti2MT.m and related routines of V. Vavryčuk were used. J.Z. was supported by the Czech Science Foundation (grant 23-06345S). E.S was supported by the HORIZON-INFRA-2024-DEV-01-01, TRANSFORM2 project.

References

Andinisari, R., K.I. Konstantinou, and P. Ranjan (2021). Seismicity along the Santorini-Amorgos zone and its relationship with active tectonics and fluid distribution, *Physics of the Earth and Planetary Interiors*, 312, 106660, https://doi.org/10.1016/j.pepi.2021.106660.

Brüstle, A. (2012). Seismicity of the eastern Hellenic Subduction Zone. *Ph.D. thesis*. Ruhr University, Bochum.

Dimitriadis, I., Papazachos, C., Panagiotopoulos, D., Hatzidimitriou, P., Bohnhoff, M., Rische, M., Meier, T., (2010). P and S velocity structures of the Santorini-Coloumbo volcanic system (Aegean Sea, Greece) obtained by non-linear inversion of travel times and its tectonic implications. *J. Volcanol. Geotherm. Res.* 195 (1), 13–30.

Evangelidis, C. P., N. Triantafyllis, M. Samios, K. Boukouras, K. Kontakos, O. J. Ktenidou, I. Fountoulakis, I. Kalogeras, N. S. Melis, O. Galanis, *et al.* (2021). Seismic Waveform Data from Greece and Cyprus: Integration, Archival, and Open Access, *Seismol. Res. Lett.* **92**, no. 3, 1672–1684, doi: 10.1785/0220200408.

Ganas., A. (2023). NOAFAULTS KMZ layer Version 5.0 (V5.0) [Data set]. Zenodo. https://doi.org/10.5281/zenodo.8075517.

Heath, B. A., Hooft, E. E. E., Toomey, D. R., Papazachos, C. B., Nomikou, P., Paulatto, M., et al (2019). Tectonism and its relation to magmatism around Santorini volcano from upper crustal *P* wave velocity. *Journal of Geophysical Research: Solid Earth*, 124, 10610–10629. https://doi.org/10.1029/2019JB017699.

Hooft, E.; Nomikou, P. and D. Toomey, (2023). Santorini Region Multibeam Synthesis, 2015. MGDS. doi:10.26022/IEDA/331252

Novotný, O., J. Zahradník, and G. A. Tselentis (2001). Northwestern Turkey earthquakes and the crustal structure inferred form surface waves observed in Western Greece, *Bull. Seismol. Soc. Am.* **91**, no. 4, 875–879, doi: 10.1785/0120000116.

Triantafyllis, N., E. Sokos, A. Ilias, and J. Zahradník (2016). Scisola: Automatic moment tensor solution for SeisComP3, *Seismol. Res. Lett.* **87**, no. 1, 157–163, doi: 10.1785/0220150065.

Triantafyllis, N., I. E. Venetis, I. Fountoulakis, E. V. Pikoulis, E. Sokos, and C. P. Evangelidis (2022). Gisola: A High-Performance Computing Application for Real-Time Moment Tensor Inversion, *Seismol. Res. Lett.* **93**, no. 2A, 957–966, doi: 10.1785/0220210153.

Vavryčuk, V. (2011). Tensile earthquakes: theory, modeling, and inversion. *J. Geophys. Res.* 116,

B12320, doi:10.1029/2011JB008770.
Waldhauser, F. (2001). HypoDD: A computer program to compute double-difference earthquake locations, *USGS Open File Rep.,* 01-113, 2001.
Waldhauser F. and W.L. Ellsworth (2000). A double-difference earthquake location algorithm: Method and application to the northern Hayward fault, *Bull. Seism. Soc. Am.*, 90, 1353-1368.
Zahradník, J., and E. Sokos (2018). ISOLA code for multiple-point source modeling –review, in *Moment Tensor Solutions - A Useful Tool for Seismotectonics*, Springer Natural Hazards, 1–28, doi: 10.1007/978-3-319-77359-9.
Zahradník, J., and E. Sokos (2025). ISOLA2024 – assessing and understanding uncertainties of full moment-tensors. *Seis. Res. Lett.,* https://doi.org/10.1785/0220240420.